# The $^{11}B(p,\alpha_0)^8Be$ reaction at sub-Coulomb energies via the Trojan-horse method

C. Spitaleri,[1,2] L. Lamia,[2,3] A. Tumino,[1,2] R. G. Pizzone,[2] S. Cherubini,[4] A. Del Zoppo,[2] P. Figuera,[2] M. La Cognata,[2,3] A. Musumarra,[1,2] M. G. Pellegriti,[1,2] A. Rinollo,[1,2] C. Rolfs,[4] S. Romano,[1,2] and S. Tudisco[1,2]
[1]*Dipartimento di Metodologie Fisiche e Chimiche per l'Ingegneria, Università di Catania, Catania, Italy*
[2]*Laboratori Nazionali del Sud-INFN, Catania, Italy*
[3]*Centro Siciliano Fisica Nucleare e Struttura della Materia, Catania, Italy*
[4]*Ruhr-Universität, Bochum, Germany*
(Received 18 December 2003; published 21 May 2004)

The $^{11}B(p,\alpha_0)^8Be$ reaction was studied from 1 MeV down to astrophysical energies by means of the Trojan-horse method applied to the $^2H(^{11}B,\alpha_o{}^8Be)n$ three-body reaction performed at an incident energy of 27 MeV. Coincidence spectra measured in a kinematically complete experiment show the presence of the quasifree $^{11}B$-$p$ process. The astrophysical factor $S(E)$ for the $^{11}B(p,\alpha_0)^8Be$ reaction was extracted from the three-body cross section at low neutron momentum. The result was compared with the behavior of the astrophysical factor from the directly measured two-body reaction.

DOI: 10.1103/PhysRevC.69.055806 PACS number(s): 26.20.+f, 21.10.Pc, 24.50.+g, 25.70.Hi

## I. INTRODUCTION

In the last decades, the improvements in the field of astrophysics observation and models have triggered nuclear reaction measurements at the astrophysical energies. Because of their crucial role in understanding the first phases of the Universe history and the subsequent stellar evolution, cross sections at the Gamow energy $E_G$ should be known with an accuracy better than 10% [1,2]. For charged particle induced reactions the Coulomb barrier $E_{CB}$, usually of the order of MeV, is much higher than $E_G$, thus implying that as the energy is lowered the reactions take place via tunneling with an exponential decrease of the cross section, $\sigma(E) \sim \exp(-2\pi\eta)$ (where $\eta$ is the Sommerfeld parameter). Owing to the strong Coulomb suppression, the behavior of the cross section at astrophysical energies is usually extrapolated from the higher energies by using the definition of the smoother astrophysical factor $S(E)$,

$$S(E) = E\sigma(E)\exp(2\pi\eta), \tag{1}$$

where $\exp(2\pi\eta)$ is the inverse of the Gamow factor, which removes the dominant energy dependence of $\sigma(E)$ due to the barrier penetrability.

Although the $S(E)$ factor allows for an easier extrapolation, large uncertainties to $\sigma(E_G)$ may be introduced due, for instance, to the presence of unexpected resonances. In order to avoid the extrapolation procedure, a number of solutions were proposed in direct measurements for enhancing the signal-to-noise ratio at astrophysical energies. However for nuclear reactions studied in laboratory, the electron clouds surrounding the interacting nuclei lead to a screened cross section $\sigma_s(E)$ larger than the "bare" nucleus one, $\sigma_b(E)$ [3–7]. Thus the enhancement factor, defined by the relation

$$f_{lab}(E) = \sigma_s(E)/\sigma_b(E) \approx \exp(\pi\eta U_e/E) \tag{2}$$

has to be taken into account. In this equation $U_e$ is the electron screening potential in the laboratory which is different from the one present in the stellar environment. In order to extract the effective cross section for stellar plasma $\sigma_{pl}(E)$, the relevant information is the bare nucleus cross section $\sigma_b(E)$ that has to be multiplied for the stellar electron screening enhancement factor $f_{pl}$, estimated within the framework of the Debye-Hückel theory. A direct measurement of $\sigma_b$ using, for instance, bare nuclei crossed beams appears almost impossible due to beam luminosity problems with such cross sections. Thus, although it is possible to measure cross sections in the Gamow energy range, the bare cross section $\sigma_b$ is extracted by extrapolating the direct data behavior at higher energies where a negligible electron screening contribution is expected.

Experimental studies of reactions involving light nuclides [8–10] have shown that the expected enhancement of the cross section at low energies was in all cases significantly larger than what could be accounted for by available atomic-physics models. This aspect deserves special attention because one may have a chance to predict the effects of electron screening in an astrophysical plasma only if it is preliminarily understood under laboratory conditions. Thus, alternative methods for determining bare nucleus cross sections of astrophysical interest are needed. In this context a number of indirect methods, e.g., the Coulomb dissociation [11,12], the ANC (asymptotic normalization coefficient) method [10–17], and the Trojan-horse method (THM) [18–34] were developed. Some of them make use of direct reaction mechanisms, such as transfer processes (stripping and pickup) and quasifree reactions (knock-out reactions). In particular, the THM is a powerful tool which selects the quasifree (QF) contribution of an appropriate three-body reaction performed at energies well above the Coulomb barrier to extract a charged particle two-body cross section at astrophysical energies free from Coulomb suppression. The THM has already been applied several times to reactions connected with fundamental astrophysical problems [35,36] such as $^{12}C(\alpha,\alpha)^{12}C$, $^7Li(p,\alpha)^4He$, $^2H(^6Li,\alpha)^4He$, $^6Li(p,\alpha)^3He$, $^3He(d,p)^4He$, $^1H(^9Be,^6Li)^4He$, and $^2H(d,p)^3H$ studied through the $^6Li(^{12}C,\alpha^{12}C)^2H$ [22], $^2H(^7Li,\alpha,\alpha)n$ [20,21,23,24,37], $^6Li(^6Li,\alpha\alpha)^4He$ [19,25,26],

 

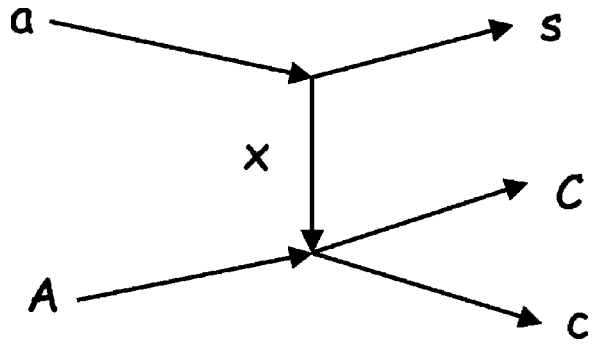


FIG. 1. Diagram representing the quasifree process $a(A,cC)s$; the particle $s$ is considered as spectator to the process, while the incident particle $A$ interacts only with the cluster $x$.

$^2$H($^6$Li,$\alpha^3$He)$n$ [27,28,38], $^6$Li($^3$He,$p\alpha$)$^4$He [30], $^2$H($^9$Be,$\alpha^6$Li)$n$ [31], and $^2$H($^6$Li,$tp$)$^4$He [32] three-body processes, respectively. Important results were obtained and those studies validated the conditions under which the method can be applied. In particular, the $^2$H($^6$Li,$\alpha^3$He)$n$ experiment [27,28] represents the first validity test of the THM where the agreement with the direct data was proven above and below the Coulomb barrier in the same data set.

The present paper reports on a recent investigation of the $^{11}$B$(p,\alpha_0)^8$Be reaction, responsible for Boron destruction in stellar environment, together with the $^{11}$B$(p,\alpha_1)^8$Be process. The extraction of a more accurate $p$-capture cross section for B may help to understand how Li, Be, and B burning takes place in stars.

The two-body $^{11}$B$(p,\alpha_0)^8$Be reaction was studied through the $^2$H($^{11}$B,$\alpha^8$Be)$n$ three-body reaction and its astrophysical $S(E)$ factor was extracted. This study allows one to perform a complete validity test of the THM below the Coulomb barrier. Indeed the $^{11}$B$(p,\alpha_0)^8$Be two-body reaction proceeds also through a state of the intermediate $^{12}$C nucleus at 16.11 MeV of excitation energy, corresponding to a resonance in the $^{11}$B-$p$ excitation function far below the Coulomb barrier [$E_{\text{c.m.}}$=0.15 MeV (where c.m.—center of mass)]. The presence of the same resonant behavior in the $^{11}$B-$p$ excitation function indirectly extracted via the THM would be a further important validity test for the method.

## II. THEORY

### A. Quasifree mechanism

The quasifree $A+a\rightarrow c+C+s$ reaction, $a$ having a strong $x\oplus s$ cluster structure, can be described by a pseudo-Feynmam diagram (Fig. 1), where only the first term of the Feynman series is retained. The upper pole in the figure describes the virtual break up of the target nucleus $a$ into the clusters $x$ and $s$; $s$ is then considered to be spectator to the $A+x\rightarrow c+C$ reaction which takes place in the lower pole. This description, called impulse approximation (IA) [39], is valid if the following hold.

(a) The momentum transfer is sufficiently high or equivalently the associated wavelength sufficiently small (less than 1 fm). Consequently the interaction can be considered confined.

(b) The incident center-of-mass energy is higher than the binding energy of the clusters $x$-$s$.

In plane wave impulse approximation (PWIA) the cross section of the three-body reaction can be factorized into two terms corresponding to the two poles of Fig. 1 [40,41] and it is given by

$$\frac{d^3\sigma}{dE_c d\Omega_c d\Omega_C} \propto \mathrm{KF}\left(\frac{d\sigma}{d\Omega}\right)|\Phi(\vec{p}_s)|^2, \tag{3}$$

where (i) $d\sigma/d\Omega$ is the off-energy-shell differential cross section for the two-body $A(x,c)C$ reaction at the center of mass energy $E_{\text{c.m.}}$ given in postcollision prescription by

$$E_{\text{c.m.}} = E_{c-C} - Q_{2\text{b}}, \tag{4}$$

where $Q_{2\text{b}}$ is the two-body $Q$-value of the $A+x\rightarrow c+C$ reaction and $E_{c-C}$ is the relative energy between the outgoing particles $c$ and $C$; (ii) KF is a kinematical factor containing the final state phase-space factor and it is a function of the masses, momenta, and angles of the outgoing particles:

$$\mathrm{KF} = \frac{\mu_{Aa} m_c}{(2\pi)^5 \hbar^7} \frac{p_C p_c^3}{p_{Aa}} \left[\left(\frac{\vec{p}_{Bx}}{\mu_{Bx}} - \frac{\vec{p}_{Cc}}{m_c}\right)\cdot\frac{\vec{p}_c}{p_c}\right]^{-1}; \tag{5}$$

(iii) $\Phi(\vec{p}_s)$ is the Fourier transform of the radial wave function $\chi(\vec{r})$ for the $x$-$s$ intercluster motion, usually described in terms of Hänkel, Eckart, and Hulthén functions depending on the $x$-$s$ system properties.

Besides the PWIA approach, the distorted wave impulse approximation (DWIA) treatment was sometimes applied in the analysis of QF reactions and QF scattering experimental data. In particular, the DWIA allows one to obtain spectroscopic information related to the intercluster wave function $\chi(\vec{r})$. In the DWIA [42] the radial wave functions are deduced from optical-model potentials so that $|\Phi(\vec{p}_s)|^2$, in Eq. (3), turns out to be dependent on the considered reaction as well as on the energy. It has to be stressed that the main difference between the momentum distributions calculated in PWIA and in DWIA is twofold [42,43].

(a) *The tails of the x-S momentum distribution.* For recoil momenta, $p_s < 100$ MeV/$c$, the essential features of $|\Phi(\vec{p}_s)|^2$ are the same in both procedures. For instance, calculations [42] of the cross section for $(p,p\alpha)$ reactions at 100 MeV on $^6$Li, $^7$Li, $^9$Be, and $^{12}$C, show very similar shapes in the low momentum region, with the only exception of $^{12}$C. However, while PWIA introduces unphysical zeros in the momentum distribution, these are properly filled in a DWIA treatment [42,44].

(b) *The absolute value of the cross section.* Indeed in the DWIA treatment the absolute value of the momentum distribution undergoes a dramatic decrease due to wave absorption effects, which are not taken into account in PWIA. The reduction factor ranges from a few units to several orders of magnitudes.

In the experimental work reported in the present paper the validity conditions of the IA appear to be fulfilled. Indeed the quite high energy of $^{11}$B of 27 MeV (740 MeV/$c$ in momentum) corresponds to an associated de Broglie wavelength of 0.26 fm, much smaller than the deuteron effective radius of

4.5 fm. We stress that in view of the various approximations involved in the THM and, in particular, of the assumption that off-energy-shell effects are negligible, one cannot extract the absolute value of the two-body cross section. However, the absolute value can be obtained through normalization to the direct data available at energies above the Coulomb barrier. Thanks to this, since we select the region of low momentum $p_s$ for the spectator ($p_s < 0$ MeV/$c$), where PWIA and DWIA wave functions have very similar shapes [44], the PWIA approach will be used for the analysis of the experimental results. Before going on with the description of the experiment, some details concerning the validity tests of the IA approach are provided. If $|\Phi(\vec{p}_s)|^2$ is known and KF is calculated, it is possible to derive $d\sigma/d\Omega$ from a measurement of $d^3\sigma/dE_c d\Omega_c d\Omega_C$:

$$\left(\frac{d\sigma}{d\Omega}\right) \propto \left[\frac{d^3\sigma}{dE_c d\Omega_c d\Omega_C}\right][\mathrm{KF}|\Phi(\vec{p}_s)|^2]^{-1}. \quad (6)$$

In particular, the value of the three-body cross section can be determined at $p_s \sim 0$ MeV/$c$ for different combinations of the quasifree reaction angles and/or different incident energies. In this case the three-body cross section divided by the kinematical factor is proportional to the off-energy-shell cross section, $\Phi(p_s \sim 0$ MeV/$c)$ being a constant.

### B. From quasifree reactions to the Trojan-horse method

The application of the quasifree mechanism to the study of reactions at astrophysical energies [29,45] derives from previous researches on this mechanism at very low energies [37,38,46–61]. This approach starts from the theory of the THM proposed by Baur [18], whose basic idea is to extract a $A+x \rightarrow C+c$ two-body reaction cross section at low energies from a suitable $A+a \rightarrow C+c+s$ three-body reaction. Under appropriate kinematical conditions, the three-body reaction is considered as the decay of the "Trojan horse" $a$ into the clusters $x$ and $s$ and the interaction of $A$ with $x$ inside the nuclear field, whereby the nucleus $s$ can be considered as a spectator during the reaction. If the bombarding energy $E_A$ is chosen high enough to overcome the Coulomb barrier in the entrance channel of the three-body reaction, both Coulomb barrier and electron screening effects are negligible.

In the original paper by Baur [18] it was proposed that the initial velocity of the projectile $A$ is compensated for by the Fermi motion of particle $x$. In this framework, a momentum of the order of hundreds of MeV/$c$ could be needed. However, in the case of $a$ nuclei with a predominant $l=0$ intercluster motion, such momenta populate the tail of the momentum distribution for particle $x$, making very critical the separation from eventual background reaction mechanisms, such as sequential decays feeding the same exit channel. Moreover, as already mentioned, the tail of the calculated momentum distribution entering Eq. (6) changes depending on the theoretical approach applied, thus a very sophisticated treatment might be required in order to get the relevant two-body cross section. In order to overcome these problems, we have introduced a different approach [19–28,30–32,45] based on the idea that the initial projectile velocity is compensated for by the binding energy of particle $x$ inside $a$. Thus the two-body reaction can be induced at very low (even vanishing) relative energy [28]. Moreover, the role of the cutoff in the momentum distribution consists in fixing the accessible astrophysical energy region, as given by

$$\Delta E_{qf} = E_{Ax} - B_{xs} \pm E_{xs}, \quad (7)$$

where $E_{Ax}$ is the beam energy in the center of mass of the two-body $A$-$x$ system, $B_{xs}$ represents the binding energy for the $x$-$b$ system, and $E_{xs}$ describes their intercluster motion within the chosen cutoff in momentum. In this way it is possible to extract the two-body cross section from Eq. (6) after inserting the appropriate penetration function $P_l$ in order to account for the penetrability effects affecting the direct data below the Coulomb barrier [28,33]. The complete formula is given by

$$\left(\frac{d\sigma}{d\Omega}\right) \propto \left[\frac{d^3\sigma}{dE_c d\Omega_c d\Omega_C}\right][\mathrm{KF}|\Phi(\vec{p}_s)|^2]^{-1} P_l. \quad (8)$$

When the projectile energy is not very high and off-energy-shell effects are not negligible, a more sophisticated approach based on a modified plane wave Born approximation [33,34] turned out to be useful since Coulomb and off-energy-shell distortions in the two-body entrance channel are included [24–28]. As shown above, since in the present experimental work the IA validity conditions are fulfilled, the more intuitive PWIA was applied for the further extraction of the two-body cross section. As already mentioned, the THM data are not affected by electron screening effects. Therefore, once the behavior of the absolute bare $S_b(E)$ factor is extracted from the two-body cross section, a model-independent estimate of the screening potential $U_e$ can be obtained from comparison with the direct screened $S(E)$ factor.

## III. EXPERIMENTAL SETUP

The experiment was performed at the Laboratori Nazionali del Sud in Catania. The SMP Tandem Van de Graaf accelerator provided a 27 MeV $^{11}B$ beam with a spot size on target of 1.5 mm and intensities up to 2–3 pnA. The relative beam energy spread was about $10^{-4}$. Deuterated polyethylene targets ($CD_2$) of about 170 $\mu$g/cm$^2$ were placed at 90° with respect to the beam direction. A silicon $\Delta E-E$ telescope, placed at a distance $d=65$ cm from the target and at $\theta=45°$ with respect to the beam axis, was used to detect the $^{11}B+^2H$ scattering yield, thus allowing for a continuous monitoring of the target thickness during the measurement. No absolute normalization was necessary for the experiment.

The detection setup consisted of a dual position sensitive detector (DPSD), made of two $5\times1$ cm$^2$, 1000 $\mu$m thick detectors, mounted one above the other and separated by 1 mm, and three $5\times1$ cm$^2$ 1000 $\mu$m thick position sensitive detectors (PSD1, PSD2, and PSD3), placed on opposite sides of the beam (Fig. 2) and covering the laboratory angles $\theta_{DPSD}=20°\pm10°$, $\theta_{PSD1}=-17°\pm7°$, $\theta_{PSD2}=-37°\pm7°$, and $\theta_{PSD3}=-57°\pm7°$, respectively.

The angular ranges were chosen in order to cover momen-

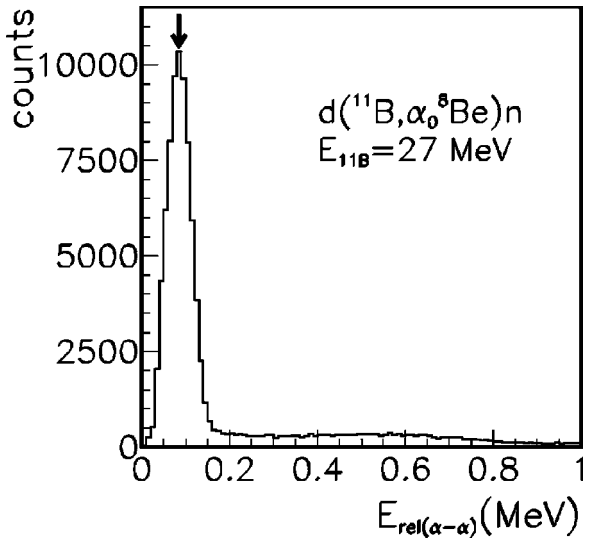


FIG. 2. Relative energy spectrum for the two coincidence particles detected in the DPSD, calculated by assuming equal masses for them. The peak at about 90 keV corresponds to the detection of two $\alpha$ particles coming from the decay of $^{8}\mathrm{Be}_{\mathrm{g.s.}}$.

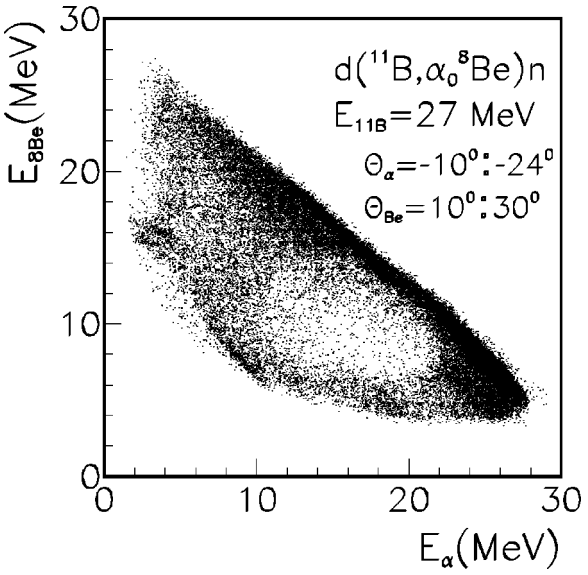


FIG. 3. $E_{^8\mathrm{Be}}$ vs $E_\alpha$ kinematic locus for the $d(^{11}\mathrm{B},{}^{8}\mathrm{Be}\alpha_0)n$ events measured at $E_0=27$ MeV.

tum values $\vec{p}_s$ of the undetected neutron *spectator* ranging from $-200$ MeV/$c$ to 200 MeV/$c$. This assures the bulk of the quasifree contributions for the breakup process of interest falling inside the investigated regions. This allowed also to cross check the method inside and outside the phase-space regions where the quasifree contribution is expected. The 1 mm separation part of the DPSD was placed in the reaction plane defined by the beam axis and the line directions connecting the center of the target with the center of the PSD's. The coplanarity of the three detectors was checked by an optical system. The solid angles covered by the detectors were $\Delta\Omega_{DPSD}=25$ msr and $\Delta\Omega_{PSD}=13.3$ msr. The $\alpha$ particles coming from the decay of $^{8}$Be were detected in coincidence in the DPSD.

The trigger for the event acquisition was given by the triple coincidences between the upper and the lower part of the DPSD and one of the three PSD's. This allowed for the kinematic identification of $^{8}$Be in the DPSD and its coincident detection with an $\alpha$ particle. Energy and position signals for the detected particles were processed by standard electronics together with the coincidence relative times.

## IV. DATA ANALYSIS AND RESULTS

### *1. Detector calibrations*

In order to perform position calibration, grids with a number of equally spaced slits were placed in front of each PSD and DPSD. A correspondence between position signal from the PSD and detection angle of the particle was then established.

Energy calibration was performed by means of a standard three-peak $\alpha$ source and $\alpha$ particles from $^{12}\mathrm{C}(^{6}\mathrm{Li},\alpha)^{14}\mathrm{N}^{*}$ and $^{2}\mathrm{H}(^{6}\mathrm{Li},\alpha)^{4}\mathrm{He}$ reactions, performed at a beam energy of 9 MeV. The total kinetic energy of the detected particles was reconstructed off-line taking into account the energy loss in the target. The overall energy and angular resolutions were found to be about 1%.

### *2. Identification of $^{8}$Be*

In order to identify $^{8}$Be, the relative energy between the two coincidence particles detected in the DPSD was calculated under the assumption of equal masses for them:

$$E_{rel}=0.5(E_{\alpha1}+E_{\alpha2}-\sqrt{E_{\alpha1}E_{\alpha2}}\cos\,\theta_{\alpha1\alpha2}). \qquad (9)$$

The relative $\theta_{\alpha1\alpha2}$ angle was deduced from the measured in-plane and the estimated mean out-of-plane angles for the two particles. The reconstructed $E_{rel}$ spectrum is shown in Fig. 2. The selection of events involving a $^{8}$Be nucleus in its ground state was performed by gating on the relevant peak around 90 keV, associated with the two $\alpha$ particles coming from its decay. From the measured energies and angles of the $\alpha$ particles, energy $E_{^8\mathrm{Be}}$ and emission angle $\theta_{^8\mathrm{Be}}$ of $^{8}\mathrm{Be}_{\mathrm{g.s.}}$ (where g.s. stands for ground state) were calculated. Due to the geometrical detection efficiency of the DPSD the contribution of the excited levels of $^{8}$Be is negligible. For this reason it is not possible to extract from this experiment the $S(E)$ factor for the $p(^{11}\mathrm{B},\alpha_1)^{8}\mathrm{Be}$ reaction. After the identification of $^{8}$Be and the assumption of mass number 4 for the third particle detected in the same coincidence event, the locus of events in $E_\alpha$ vs. $E_{^8\mathrm{Be}}$ for the $^{2}\mathrm{H}(^{11}\mathrm{B},\alpha_0{}^{8}\mathrm{Be})n$ reaction (Fig. 3) was compared with the corresponding three-body kinematic calculation, appearing to be very well reconstructed. The $Q$-value spectrum for the coincidence events is reported in Fig. 4. The peak centered at about 6 MeV corresponds to the three-body reaction of interest whose $Q$ value is 6.36 MeV. Events inside this peak were selected for further analysis.

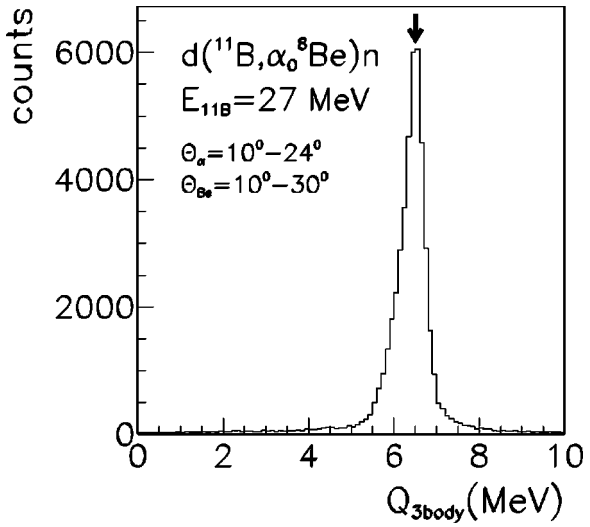


FIG. 4. $Q$-value spectrum corresponding to the kinematic locus of Fig. 3. The sharp peak, around 6 MeV, corresponds to the $^8Be+\alpha+n$ channel.

### A. Experimental evidence of quasifree mechanism

#### *1. Relative energy two-dimensional plots*

After the selection of the $^8Be_{g.s.}+\alpha+n$ channel, the next step of data analysis was to examine if in the considered experimental kinematic regions, the contribution of the quasifree process to the overall $^8Be_{g.s.}$-$\alpha$ coincidences was evident and well separated from others. As already mentioned, the analysis of the experimental results is in general complicated by the presence of other reaction mechanisms producing the same particles in the final state, e.g., sequential decay (SD) and direct break-up. In order to study the nature of the events belonging to the kinematic locus for the $^2H(^{11}B,^8Be\alpha_0)n$ reaction (Fig. 3), relative energies for any two of the three final particles were obtained. Figures 5(a) and 5(b) show coincidence events in the $^8Be_{g.s.}$-$n$ vs. $^8Be_{g.s.}$-$\alpha$ and $\alpha$-$n$ vs. $^8Be_{g.s.}$-$\alpha$ relative energy planes. These representations show very clear vertical loci, corresponding to levels at excitation energies of 9.6, 10.84, and 16.11 MeV in $^{12}C$ [vertical loci in both Figs. 5(a) and 5(b)]. Much less defined loci associated with the 2.43 and 3.30 MeV states in $^9Be$ [horizontal loci of Fig. 5(a), corresponding to diagonal loci of Fig. 5(b)] and with the ground states of $^5He$ [horizontal locus of Fig. 5(b)] can be recognized. From such a comprehensive analysis of the relative energy two-dimensional plots, where the resolution appears to be better than the experimental one due to the well-known lens effect [11], it comes out that the reaction $^{11}B(p,\alpha_0)^8Be$ mainly proceeds through formation of an intermediate $^{12}C$ excited nucleus with a much weaker contribution from states of $^9Be$ and $^5He$. However, the decays from $^5He$ and $^9Be$ intermediate states leave the final neutron with a momentum larger than 80 MeV/$c$, and only the 16.11 MeV state of $^{12}C$ can contribute within the astrophysical region, the other two $^{12}C$ states being below the $^{11}B+p$ decay threshold. The "noise" contribution connected to SD from the 16.11 MeV state of $^{12}C$ has to be discriminated against in the following data analysis.

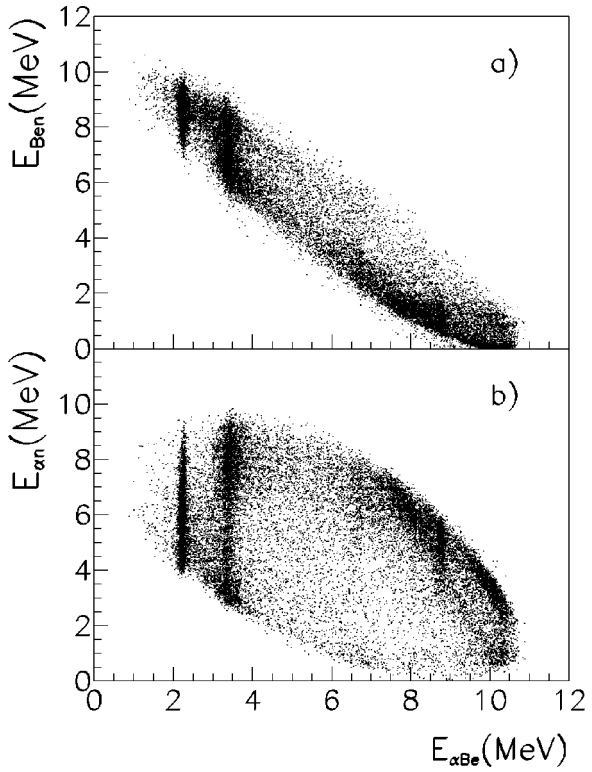


FIG. 5. (a) $^8Be_{g.s.}$-$\alpha$ vs $^8Be_{g.s.}$-$n$ and (b) $^8Be_{g.s.}$-$\alpha$ vs $\alpha$-$n$ relative energy two-dimensional plot. Very clear vertical loci appear, corresponding to excited states of $^{12}C$ (see text for details).

#### *2. Study of angular correlation spectra*

Before any data extraction the next step is that of studying the reaction mechanism involved in the population of the $^{12}C$ state at 16.11 MeV of excitation energy. The same state can be populated via quasifree mechanism or via sequential decay as sketched in Figs. 6(a) and 6(b). A way to investigate the reaction mechanisms and therefore the nature (QFR or SD) of this level is that of performing the angular correlation analysis on the data. Figure 7 shows typical coincidence spectra projected on $E_\alpha$ axis for a fixed $\theta_{^8Be}$ and for different

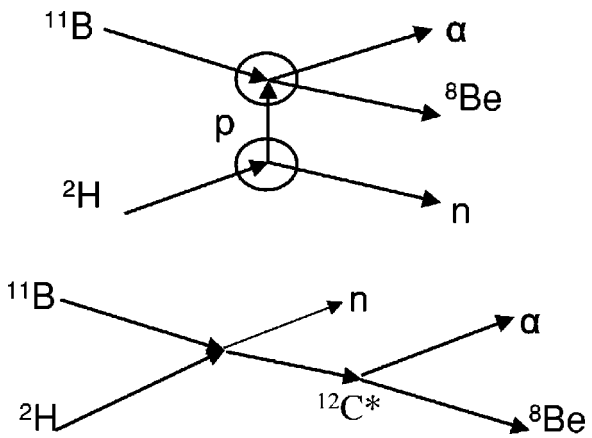


FIG. 6. Simplified scheme for the (a) quasifree $^{11}B(d,\alpha_0{}^8Be)n$ reaction; (b) a possible competitive $^{11}B(d,n)^{12}C^*(\alpha_0{}^8Be)$ sequential decay feeding the same final channel.

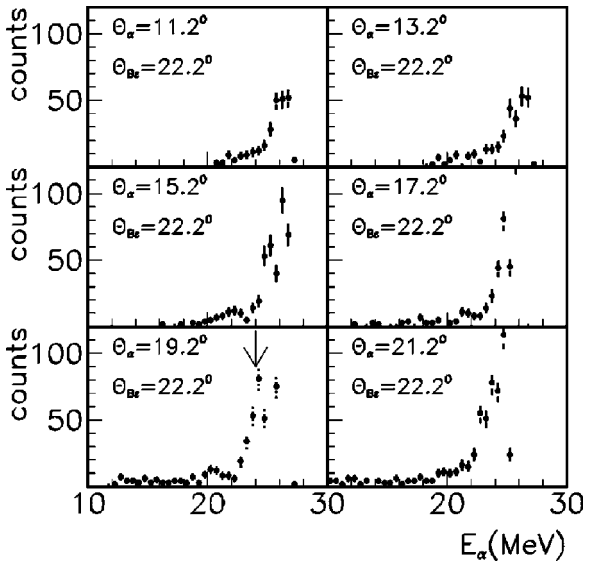


FIG. 7. Typical coincidence spectra projected on the $E_\alpha$ axis for a fixed $\theta_{\mathrm{Be}}$ and different $\theta_\alpha$, within the angular ranges of ±1°. The condition corresponding to deuteron momentum $p_n=0$ MeV/$c$ is marked with an arrow.

$\theta_\alpha$ angles within the experimental angular range. From the sequence of these spectra it can be observed that the coincidence yield attains a maximum when the neutron momentum approaches zero value. The condition of nearly zero neutron momentum is marked with an arrow in the figure. This feature is expected for a quasifree reaction because the momentum distribution of *n*-*p* system in the deuteron nucleus has a maximum for $p_n=0$ MeV/$c$. The $\theta_{^8\mathrm{Be}},\theta_\alpha$) angles corresponding to this condition represent the so called quasifree angles. Similar results were obtained for other quasifree angle pairs. This represents a first necessary check for the existence of the quasifree mechanism in the $^2\mathrm{H}(^{11}\mathrm{B},\alpha_0{}^8\mathrm{Be})n$ reaction.

#### *3. Data as a function of the neutron momentum $p_n$*

A complementary way to test the presence of QF and/or SD mechanisms is to investigate the correlation between the $E_{^8\mathrm{Be}\text{-}\alpha}$ relative energy and the momentum $p_n$ for all coincidence events, in the whole angular range covered by the detectors. The $E_{^8\mathrm{Be}\&\#2010;\alpha}$ vs. $p_n$ two-dimensional plot (Fig. 8) shows that the main contribution of the already mentioned 16.11 MeV state of $^{12}$C is confined in the $|p_n|\leqslant 40$ MeV/$c$ range corresponding to the QF region. Moreover, in order to explore the behavior of the coincidence yield depending on the momentum $p_n$, relative energy $E_{^{11}\mathrm{B}\text{-}p}$ spectra [$E_{^{11}\mathrm{B}\text{-}p}$ corresponds to the $E_{\mathrm{c.m.}}$ variable of Eq. (4)] divided by the phase-space contribution were reconstructed for different ranges of the neutron momentum $p_n$. Within $0\ \mathrm{MeV}/c \leqslant |p_n| \leqslant 20\ \mathrm{MeV}/c$ [Fig. 9(a)] and $20\ \mathrm{MeV}/c \leqslant |p_n| \leqslant 40\ \mathrm{MeV}/c$ [Fig. 9(b)] momentum ranges, the coincidence yield appears to be quite high, in particular, close to the $E_{^{11}\mathrm{B}\text{-}p}$ resonant window. Moving a bit further in momentum, the coincidence yield decreases as shown in Fig. 9(c) ($40\ \mathrm{MeV}/c \leqslant |p_n| < 60\ \mathrm{MeV}/c$), where the larger error bars are due to the lower statistics. Events with a $|p_n| > 60$ MeV/$c$ were excluded from the correlation analysis since, as already mentioned, they contain the contribution from sequential decays of $^5$He and $^9$Be intermediate states.

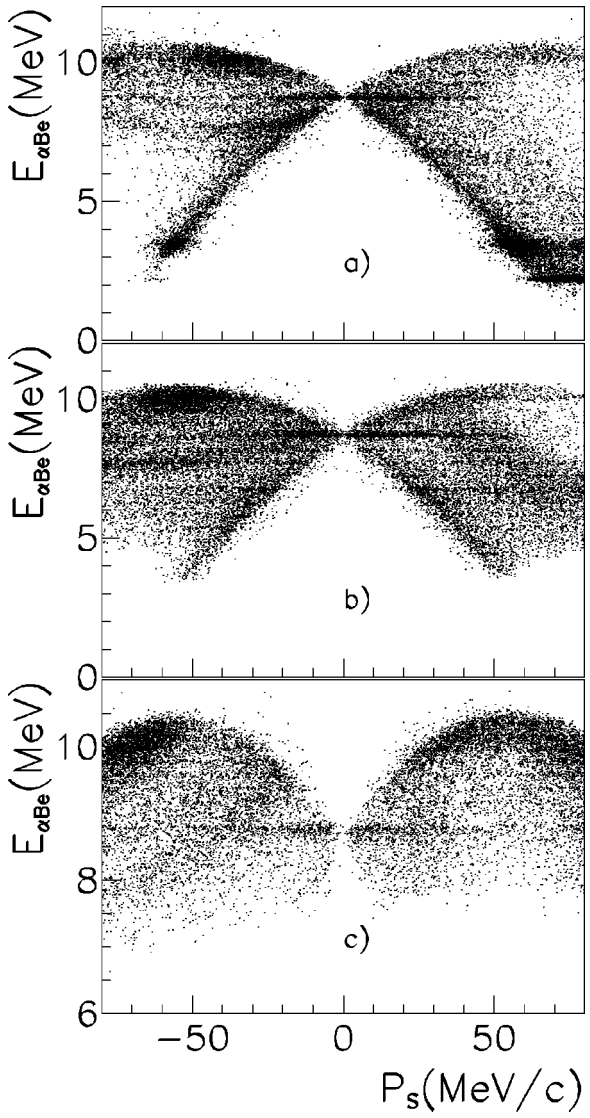


FIG. 8. $E_{\mathrm{Be}\text{-}\alpha}$ relative energy as a function of the spectator momentum $p_n$. The sharp line at 8.7 MeV in the region of low $p_n$ is associated with the 16.11 MeV excited state of $^{12}$C.

These experimental data provide further evidence for a strong correlation between coincidence yield and neutron momentum $p_n$, a necessary condition for the dominance of the quasifree mechanism in the region approaching zero neutron momentum. But in case of a resonance within the low $p_n$ region this result might not be a sufficient condition, since the manifested correlation can partially depend on the resonant behavior, regardless of its SD or QF origin.

#### *4. Analysis of the neutron momentum distribution*

An observable which turns out to be more sensitive to the reaction mechanism is the shape of the experimental momentum distribution. In order to reconstruct the experimental $p_n$ distribution, the energy sharing method [53] was applied to each pair of coincidence detectors selecting $^{11}\mathrm{B}+p$ relative

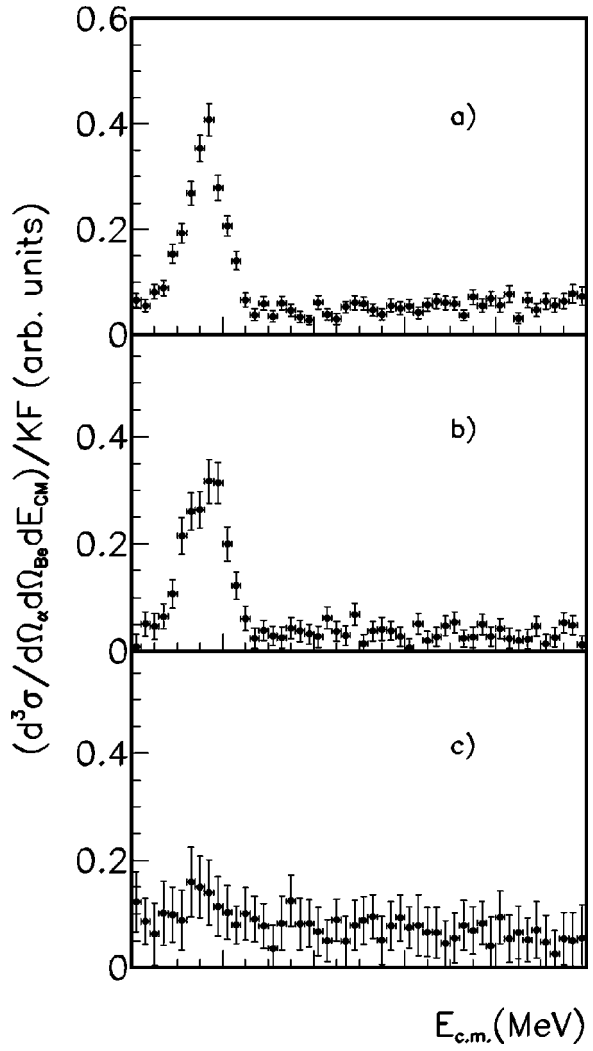


FIG. 9. Three-body cross section for different $p_n$ ranges: (a) 0 MeV/$c \leqslant |p_n| \leqslant 20$ MeV/$c$, (b) 20 MeV/$c \leqslant |p_n| \leqslant 40$ MeV/$c$, and (c) 40 MeV/$c \leqslant |p_n| \leqslant 60$ MeV/$c$.

energy windows of 100 keV. Dividing the resulting three-body coincidence yield by the kinematic factor, this gives a quantity which is proportional to the product of the $p_n$ momentum distribution with the differential $^{11}B$-$p$ two-body cross section [see Eq. (6)]. Within such restricted $^{11}B+p$ relative energy ranges, the differential two-body cross section of the $^{11}B$-$p$ reaction, can be considered constant. Thus the quantity defined above and reported in Fig. 10, represents the experimental $p_n$ momentum distribution in arbitrary units. The error bars include only the statistical errors. The extracted experimental momentum distribution (Fig. 10) was then compared with the theoretical one, given in terms of a Hulthén wave function in momentum space:

$$\Phi(\vec{p}_s) = \frac{1}{\pi}\sqrt{\frac{ab(a+b)}{(a-b)^2}}\left[\frac{1}{a^2+p_s^2} - \frac{1}{b^2+p_s^2}\right] \qquad (10)$$

with parameters $a=0.2317$ fm$^{-1}$ and $b=1.202$ fm$^{-1}$ [37] for the deuteron ground state. The theoretical distribution was superimposed on the data of Fig. 10, after being normalized

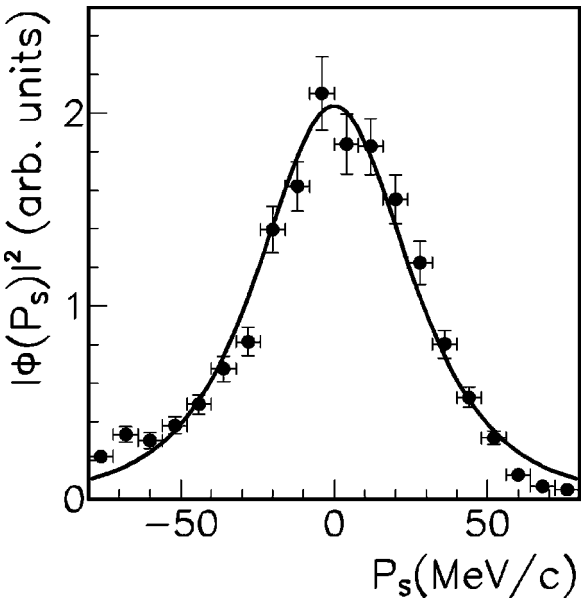


FIG. 10. Experimental momentum distribution (full dots) compared with the theoretical one given in terms of a Húlthen function (full line).

to the experimental maximum. Equation (10) with parameters $a$ and $b$ from Ref. [37] reproduces quite well the shape of experimental data. At the end of this first step of data analysis we can conclude with the following points.

(a) In the experimentally selected kinematic regions, the QF mechanism gives the main contribution to the $^{11}B+d$ reaction at 27 MeV.

(b) The QF mechanism is selected, without significant contribution from contaminant SD processes.

(c) The analysis in PWIA can be used to describe the process.

### B. From the quasifree coincidence data to the indirect two-body cross section

#### *1. Selection of the quasifree mechanism*

In order to select the region where the QF mechanism is dominant, coincidence events for neutron momentum ranging between −40 MeV/$c$ and 40 MeV/$c$ were considered in the subsequent analysis. A Monte Carlo calculation was then performed to extract the $[KF|\Phi(\vec{p}_s)|^2]$ product. The momentum distribution entering the calculation was that given in Eq. (10). The geometrical efficiency of the experimental setup as well as the detection thresholds of the PSD's were taken into account. An error calculation for the relative energies $E_{^8Be\text{-}\alpha}$ was also performed, leading to an average value of about 40 keV. Following the PWIA prescription of Eq. (6), the two-body cross section $d\sigma/d\Omega$ was derived by dividing the selected three-body coincidence yield by the result of the Monte Carlo calculation. As already mentioned, since this approach provides the off-energy-shell two-body cross section, it is necessary to perform the appropriate validity tests for the adopted IA.

#### *2. Angular distributions: First validity test*

A first test makes a comparison between the indirectly extracted angular distributions and the direct behavior. The

relevant angle in order to get the indirect angular distributions, i.e., the emission angle for the $\alpha$-particle in the $\alpha$-$^8$Be center-of-mass system, can be calculated according to the relation [43]

$$\theta_{\mathrm{c.m.}} = \arccos\frac{(\mathbf{v_p} - \mathbf{v_t}) \cdot (\mathbf{v_C} - \mathbf{v}_\alpha)}{|\mathbf{v_p} - \mathbf{v_t}||\mathbf{v_C} - \mathbf{v}_\alpha|}$$

where the vectors $\mathbf{v_p}$, $\mathbf{v_t}$, $\mathbf{v_C}$, and $\mathbf{v}_\alpha$ are the velocities of projectile, transferred proton, and the outgoing $^8$Be and $\alpha$ particles, respectively. These quantities can be calculated from their corresponding momenta in the lab system, where the momentum of the transferred particle is equal and opposite to that of the spectator neutron (quasifree assumption) [43]. The center-of-mass angular ranges covered in the present experiment were $\theta_{\mathrm{c.m.}}=120°-160°$, $\theta_{\mathrm{c.m.}}=75°-120°$, and $\theta_{\mathrm{c.m.}}=20°-60°$, respectively, for DPSD-PSD1, DPSD-PSD2, and DPSD-PSD3 coincidences. The angular distribution test was performed for each set of coincidence events spanning the full $^8$Be-$\alpha$ relative energy range in steps of $\Delta E_{\mathrm{c.m.}}=200$ keV. The angular distributions were then normalized to the direct data from Ref. [62] within the corresponding angular ranges and compared with them. An example of the results is shown in Fig. 11. The error bars include both statistical and normalization errors and the two-body cross section is in arbitrary units. The solid lines show the behavior of the direct angular distributions [62] integrated in the same energy bins. The quite fair agreement between the two trends makes us confident on the validity of the IA.

#### *3. Excitation functions: Second validity test*

A second validity test applies to the behavior of the indirect excitation function. It has to be verified that the behavior of the off-energy-shell two-body cross section integrated over the full experimental $\theta_{\mathrm{c.m.}}$ range covered is consistent with that of direct data within the same angular region. Since the investigated $^{11}$B-$p$ relative energy region lies below the Coulomb barrier ($B_C=1.7$ MeV), and, as foreseen, the extracted THM two-body cross section is free of Coulomb suppression, in order to do the comparison indirect data were multiplied by the Coulomb penetration function as given in Refs. [28,33], assuming a dominant $l=0$ partial wave in the entrance channel of the $^{11}$B-$p$ two-body reaction. The resulting two-body cross section is shown in Fig. 12 (full dots), where direct data from Ref. [62] are also reported (open symbols). The normalization to the direct behavior was performed in the region $E_{^{11}\mathrm{B}\text{-}p}=800-900$ keV. A good agreement between the two data sets shows up, revealing that the assumption for a dominant $l=0$ partial wave is correct within the accuracy of the experimental information available. Moreover, it has to be stressed that this agreement is indeed a necessary condition for the further extraction of the astrophysical $S(E)$ factor by means of THM [19–22,25,28]. At the end of this second test on the data we can conclude that the validity of the pole approximation for this experiment is verified. Moreover, both tests confirm that the PWIA analysis is able to correctly describe the studied process.

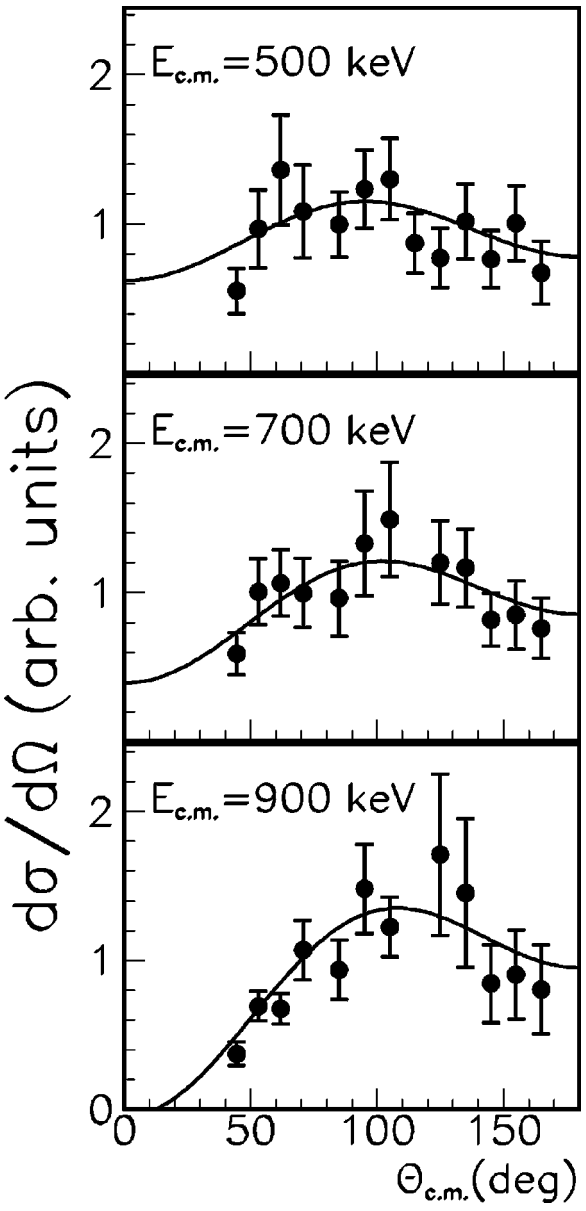


FIG. 11. Example of angular distributions showing the $^{11}$B-$p$ differential cross section as a function of $\theta_{\mathrm{c.m.}}$ (see text for details). The $^{11}$B-$p$ relative energy range is covered in steps of $\Delta E_{\mathrm{c.m.}}=200$ keV.

### C. Astrophysical factor

The procedure to derive the astrophysical $S(E)$ factor from our data employs the usual definition of Eq. (1). Since the experimental angular distributions appear to be quite flat at these low energies, their behavior was easily extrapolated to the $\theta_{\mathrm{c.m.}}$ regions $0°-20°$ and $160°-180°$ not covered in the experiment. Then the indirect two-body cross section was integrated in the full $\theta_{\mathrm{c.m.}}=0°-180°$ angular range, and inserted in Eq. (1) in order to get the $S(E)$ factor. Figure 13 shows the extracted $S(E)$ factor compared with the direct one, both averaged out at the same energy bin of 20 keV. There is a fair agreement in the energy region $E_{\mathrm{c.m.}}>100$ keV. Also the resonance corresponding to the mentioned 16.11 MeV state of $^{12}$C, which dominates the

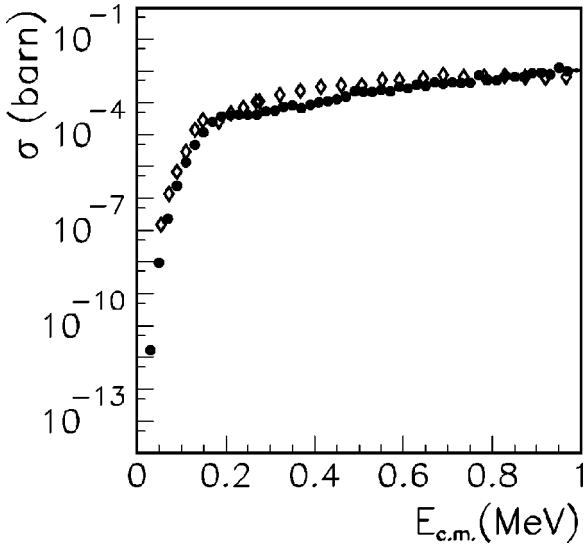


FIG. 12. Comparison between the indirect excitation function (full dots) for the $^{11}B(p,\alpha)^8Be_{g.s.}$ reaction and the direct behavior (open symbols) [62].

cross section at low energy, is well reproduced. A fit to the indirect data was performed by using the following parametrization:

$$S_b(E) = 0.31 + 3.00E - 2.28E^2 + 3.60\ \exp\left[-0.5\left(\frac{E-0.16}{0.06}\right)^2\right], \qquad (11)$$

where the Gaussian function accounts for the resonant behavior. The full line in Fig. 14, superimposed on the indirect data, represents the result of the fit. The extracted bare $S(0)$ value turns out to be $S_b(0)=(0.41\pm0.09)$ MeV b, where the quoted uncertainty accounts also for a systematic error of about ~20%. In the work of Becker *et al.* [62] a larger value of $S_b(0)\approx 2.1$ MeV b is extrapolated from the higher energy region. A recent *R*-matrix fit on the direct data [63] gives $S_b(0)=2.4$ MeV b. A possible explanation for the discrepancy observed in the two values of the $S_b(E)$ factor, namely, the one obtained in the present work and that extrapolated from direct measurements [62,63], might be ascribed to uncertainties deriving from the extrapolation procedure on the direct data or to the penetrability corrections in the very low energy region, which produce an excessive decrease of the lowest energy indirect points. The lack of direct data below 40 keV does not help in defining the "transition" region where screening effects start to be important, and prevents us from extracting the screening potential.

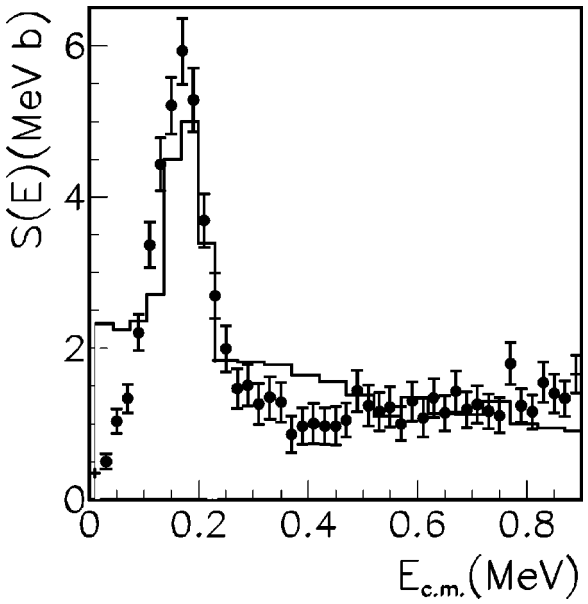


FIG. 13. Extracted $S(E)$ factor (full dots) compared with the direct one [62] (histogram line), both averaged out at the same energy bin of 20 keV.

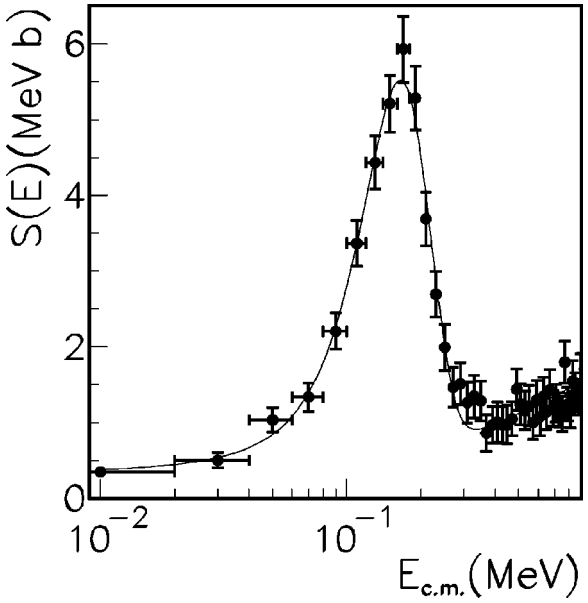


FIG. 14. Indirect astrophysical $S(E)$ factor (full dots) with superimposed the result of a polynomial fit (full line) performed on the data and discussed in the text.

## V. CONCLUSIONS

The indirect study of the $^{11}B(p,\alpha_0)^8Be$ reaction was performed from 1 MeV down to the astrophysical region applying the THM to the $^2H(^{11}B,\alpha_0{}^8Be)n$ three-body breakup process. The results confirm the presence of a strong quasi-free contribution populating the three-body channel around the region of nearly zero spectator momentum. The mechanism proceeds through a virtual two-body reaction of the incident $^{11}B$ with the proton in $^2H$. For the first time the validity test of the THM based on the behavior of the angular distributions could be performed. Both angular distributions and excitation function indirectly extracted agree with the direct behavior in the region where screening effects are negligible. The extracted bare $S_b(0)$ value appears to be about a factor 6 lower than that extrapolated from direct data. The disagreement is still not understood and further study is needed. Because of this and due to the lack of direct data

below 40 keV, the THM could not be applied for an estimate of the effects of the electron screening for the $^{11}$B-$p$ system. Direct data are missing because of the very low cross sections involved in the $^{11}B(p,\alpha_0)^8Be$ reaction. From the astrophysical point of view the $p$-capture reaction rate on $^{11}$B is dominated by the $^{11}B(p,\alpha_1)^8Be$ reaction, whose cross section is about two orders of magnitude higher. The indirect measurement of this reaction would allow us to evaluate the electron screening potential. However, experimental setups with segmented detectors covering larger solid angles are needed in order to detect the $\alpha$ particles coming from the decay of $^8Be^*$.

In conclusion, a point to be stressed is that the experiments we are dealing with using the THM can be performed in a relatively short time with very simple experimental setups and low intensity beams. Moreover, under special conditions supporting the validity of IA, the PWIA can be used to extract the two-body cross sections. In any case more sophisticated approaches based on the DWBA [24,28,33,34] can be applied. It is worth noticing also that in many THM experiments where the IA factorization was successfully applied, the spectator particle was a neutron inside the deuteron. It would be highly desirable to study the same two-body processes by using different Trojan-horse nuclei. This would allow us to test the validity of the factorization against effects such as the Coulomb distortion due to the spectator particle, as well as the bound structure of the Trojan-horse nucleus. In the future, $p$-capture reactions, such as $^{11}B(p,\alpha)^8Be$, $^7Li(p,\alpha)^4He$, and $^6Li(p,\alpha)^3He$, already studied via the THM off the neutron in $^2$H, are planned to be investigated using $^3$He as the Trojan horse.

It has to be emphasized that the described analysis procedure for the applicability of the THM is standard and thus all the validity tests performed in the present paper have to be repeated whenever the THM is applied [19–21,23–26,28,37]. A lot remains to be done in order to achieve reliable information for many key reactions and processes. This would allow also to understand off-energy-shell effects in the THM. Furthermore the electron screening effect needs to be investigated in more details in view of its prospective role in the framework of energy production in fusion reactors.

## ACKNOWLEDGMENTS

The authors would like to thank Professor M. Lattuada for his helpful collaboration during the course of the experiment and Professor R. Siemssen for his fruitful comments. They also thank the technical staff of the Laboratori Nazionali del Sud for their invaluable assistance.

[1] C. Rolfs and W. S. Rodney, *Cauldrons in the Cosmos* (University of Chicago Press, Chicago, 1988).
[2] C. Rolfs, Prog. Part. Nucl. Phys. **153**, 23 (2001).
[3] H. J. Assenbaum, K. Langanke, and C. Rolfs, Z. Phys. A **327**, 461 (1987).
[4] F. Streider, C. Rolfs, C. Spitaleri, and P. Corvisiero, Naturwissenschaften **88**, 461 (2001).
[5] C. Casella *et al.*, Luna Collaboration, Nucl. Phys. **A706**, 203 (2002).
[6] R. Bonetti, C. Broggini, L. Campaiola, P. Corvisiero, A. D'Alessandro, M. Dessalvi, A. D'Onofrio, A. Fubini, G. Gervino, L. Gialanella, U. Greife, A. Guglielmetti, C. Gustavino, G. Imbriani, M. Junger, P. Prati, V. Roca, C. Rolfs, M. Romano, F. Schuemann, F. Streider, F. Terrasi, H. P. Trautvetter, and S. Zavatarelli, Phys. Rev. Lett. **82**, 5205 (1999).
[7] M. Junker, A. D'Alessandro, S. Zavatarelli, C. Arpesella, E. Bellotti, C. Broggini, P. Corvisiero, G. Fiorentini, A. Fubini, G. Gervino, U. Greife, C. Gustavino, J. Lambert, P. Prati, W. S. Rodney, C. Rolfs, F. Streider, H. P. Trautvetter, and D. Zahnow, Phys. Rev. C **57**, 2700 (1998).
[8] S. Engstler *et al.*, Phys. Lett. B **202**, 179 (1988).
[9] S. Engstler *et al.*, Phys. Lett. B **279**, 20 (1992).
[10] R. Bonetti *et al.*, Phys. Rev. Lett. **82**, 5205 (1999).
[11] G. Baur and H. Rebel, J. Phys. G **20**, 1 (1994), and references therein.
[12] G. Baur and H. Rebel, Annu. Rev. Nucl. Part. Sci. **46**, 321 (1996).
[13] X. D. Tang, A. Azhari, C. A. Gagliardi, A. M. Mukhamedzhanov, F. Pirlepeson, L. Trache, R. E. Tribble, V. Burjan, V. Kroha, and F. Castiou, Phys. Rev. C **67**, 015804 (2003).
[14] A. M. Mukhamedzhanov, C. A. Gagliardi, and R. E. Tribble, Phys. Rev. C **63**, 024612 (2001).
[15] A. Azhari, V. Burjan, F. Carstoiu, C. A. Gagliardi, V. Kroha, A. M. Mukhamedzhanov, F. M. Nunes, X. Tang, L. Trache, and R. E. Tribble, Phys. Rev. C **63**, 055803 (2001).
[16] A. M. Mukhamedzhanov and R. E. Tribble, Phys. Rev. C **59**, 3418 (1999).
[17] A. M. Mukhamedzhanov, A. M. Clark, C. A. Gagliardi, Y. W. Lui, L. Trache, R. E. Tribble, H. M. Xu, V. Cejpek, V. Burjan, V. Kroha, and F. Castiou, Phys. Rev. C **56**, 1302 (1997).
[18] G. Baur, Phys. Lett. B **178**, 135 (1986).
[19] S. Cherubini, V. N. Kondratyev, M. Lattuada, C. Spitaleri, Dj. Miljanić, M. Zadro, and G. Baur, Astrophys. J. **457**, 855 (1996).
[20] G. Calvi, S. Cherubini, M. Lattuada, S. Romano, C. Spitaleri, M. Aliotta, G. Rizzari, M. Sciuto, R. A. Zappalà, V. N. Kondratyev, Dj. Miljanić, M. Zadro, G. Baur, O. Yu. Goryunov, and A. A. Shvedov, Nucl. Phys. **A621**, 139c (1997).
[21] C. Spitaleri, M. Aliotta, S. Cherubini, M. Lattuada, Dj. Miljanić, S. Romano, N. Soić, M. Zadro, and R. A. Zappalà, Phys. Rev. C **60**, 055802 (1999).
[22] C. Spitaleri, M. Aliotta, P. Figuera, M. Lattuada, R. G. Pizzone, S. Romano, A. Tumino, C. Rolfs, L. Gialanella, F. Strieder, S. Cherubini, A. Musumarra, Dj. Miljanić, S. Typel, and H. H. Wolter, Eur. Phys. J. A **7**, 181 (2000).
[23] A. Aliotta, C. Spitaleri, M. Lattuada, A. Musumarra, R. G. Pizzone, A. Tumino, C. Rolfs, and F. Strieder, Eur. Phys. J. A **9**, 435 (2000).
[24] M. Lattuada, R. G. Pizzone, S. Typel, P. Figuera, Dj. Miljanić, A. Musumarra, M. G. Pellegriti, C. Rolfs, C. Spitaleri, and H.

H. Wolter, Astrophys. J. **562**, 1076 (2001).
[25] C. Spitaleri, S. Typel, R. G. Pizzone, M. Aliotta, S. Blagus, M. Bogovac, S. Cherubini, P. Figuera, M. Lattuada, M. Milin, Dj. Miljanić, A. Musumarra, M. G. Pellegriti, D. Rendić, C. Rolfs, S. Romano, N. Soić, A. Tumino, H. H. Wolter, and M. Zadro, Phys. Rev. C **63**, 055801 (2001).
[26] A. Musumarra, R. G. Pizzone, S. Blagus, M. Bogovac, P. Figuera, M. Lattuada, M. Milin, Dj. Miljanić, M. G. Pellegriti, D. Rendić, C. Rolfs, S. Soić, C. Spitaleri, S. Typel, H. H. Wolter, and M. Zadro, Phys. Rev. C **64**, 068801 (2001).
[27] A. Tumino, C. Spitaleri, A. Di Pietro, P. Figuera, M. Lattuada, A. Musumarra, M. G. Pellegriti, R. G. Pizzone, S. Romano, C. Rolfs, S. Tudisco, and S. Typel, Nucl. Phys. **A718**, 499 (2003).
[28] A. Tumino, C. Spitaleri, A. Di Pietro, P. Figuera, M. Lattuada, A. Musumarra, M. G. Pellegriti, R. G. Pizzone, S. Romano, C. Rolfs, S. Tudisco, and S. Typel, Phys. Rev. C **67**, 065803 (2003).
[29] C. Spitaleri, S. Cherubini, A. Del Zoppo, A. Di Pietro, P. Figuera, M. Gulino, M. Lattuada, Dj. Miljanić, A. Musumarra, M. G. Pellegriti, R. G. Pizzone, C. Rolfs, S. Romano, S. Tudisco, and A. Tumino, Nucl. Phys. **A719**, 99 (2003).
[30] M. La Cognata, A. Musumarra, C. Spitaleri, S. Cherubini, A. Del Zoppo, P. Figuera, L. Lamia, L. Pappalardo, M. G. Pellegriti, A. Rinollo, R. G. Pizzone, C. Rolfs, S. Romano, D. Schürmann, F. Strieder, S. Tudisco, A. Tumino, and S. Typel, LNS-INFN Activity Report 2002.
[31] R. G. Pizzone, C. Li, C. Spitaleri, S. Cherubini, P. Figuera, M. Gulino, M. La Cognata, L. Lamia, A. Musumarra, M. G. Pellegriti, S. Romano, A. Tumino, and S. Tudisco, LNS-INFN Activity Report 2002 (Ref. [30]).
[32] A. Rinollo, S. Romano, C. Spitaleri, S. Cherubini, A. Del Zoppo, P. Figuera, M. La Cognata, M. Lattuada, A. Musumarra, M. G. Pellegriti, R. G. Pizzone, S. Tudisco, and A. Tumino, LNS-INFN Activity Report 2002.
[33] S. Typel and H. Wolter, Few-Body Syst. **29**, 7 (2000).
[34] S. Typel and G. Baur, Ann. Phys. (N.Y.) **305**, 228 (2003).
[35] C. J. Copi, D. N. Schramm, and M. S. Turner, Scand. J. Immunol. **627**, 192 (1995).
[36] L. Piau and S. Turck-Chieze, Astrophys. J. **566**, 419 (2002).
[37] M. Zadro, Dj. Miljanić, C. Spitaleri, G. Calvi, M. Lattuada, and F. Riggi, Phys. Rev. C **40**, 181 (1989).
[38] G. Calvi, M. Lattuada, Dj. Miljanić, F. Riggi, C. Spitaleri, and M. Zadro, Phys. Rev. C **41**, 1848 (1990).
[39] G. F. Chew, Phys. Rev. **80**, 196 (1950).
[40] U. G. Neudatchin and Y. F. Smirnov, At. Energy Rev. **3**, 157 (1965).
[41] G. Jacob, and Th. A. Maris, Rev. Mod. Phys. **38**, 121 (1966).
[42] P. G. Roos, N. S. Chant, D. A. Goldberg, H. D. Holdgren, and R. Woody, III, Phys. Rev. C **15**, 69 (1977), and references therein.
[43] M. Jain, P. G. Roos, H. G. Pugh, and H. D. Holgrem, Nucl. Phys. **A153**, 49 (1970).
[44] N. S. Chant and P. G. Roos, Phys. Rev. C **15**, 57 (1977), and references therein.
[45] C. Spitaleri, *Problems of Fundamental Modern Physics II* (World Scientific, Singapore, 1990), pp. 21–35.
[46] A. K. Jain, J. Y. Grossiodor, M. Chevalier, P. Gaillard, A. Guichard, M. Gusakow, and J. P. Pizzi, Nucl. Phys. **A216**, 519 (1973).
[47] A. Guichard, M. Chevalier, P. Gaillard, J. Y. Grossiodor, M. Gusakow, J. P. Pizzi, and C. Rula, Phys. Rev. C **4**, 700 (1971).
[48] M. Furic, R. K. Cole, H. H. Forster, C. C. Kim, D. Y. Park, J. Rucker, H. Spizer, and C. N. Weddell, Phys. Lett. **39B**, 629 (1972).
[49] Dj. Miljanić, T. Zabel, R. B. Lambert, and G. C. Phillips, Nucl. Phys. **A215**, 221 (1973).
[50] Dj. Miljanić, J. Hudomalj, G. S. Mutchler, E. Andrade, and G. C. Phillips, Phys. Lett. **50B**, 330 (1974).
[51] J. Kasagi, T. Nakagawa, N. Sekine, and T. Tohei, Nucl. Phys. **A239**, 233 (1975).
[52] I. Slaus, R. G. Allas, L. Beach, R. O. Bondelid, E. L. Petersen, J. M. Lambert, P. A. Taedo, and A. Molyle, Nucl. Phys. **A286**, 67 (1977).
[53] N. Arena, D. Vinciguerra, F. Riggi, and C. Spitaleri, Nuovo Cimento Soc. Ital. Fis., A **45**, 405 (1978).
[54] M. Lattuada, F. Riggi, C. Spitaleri, D. Vinciguerra, S. Micheletti, and A. Pantaleo, Nuovo Cimento Soc. Ital. Fis., A **62**, 165 (1981).
[55] M. Lattuada, F. Riggi, C. Spitaleri, D. Vinciguerra, C. M. Sutera, and A. Pantaleo, Nuovo Cimento Soc. Ital. Fis., A **69**, 1 (1982).
[56] M. Zadro, S. Blagus, Dj. Miljanić, M. Lattuada, F. Riggi, and C. Spitaleri, Z. Phys. A **325**, 119 (1986).
[57] M. Lattuada, F. Riggi, C. Spitaleri, D. Vinciguerra, Dj. Miljanić, M. Zadro, and Yao Jinzhang, Nucl. Phys. **A458**, 493 (1986).
[58] M. Zadro, Dj. Miljanić, M. Lattuada, F. Riggi, and C. Spitaleri, Nucl. Phys. **A474**, 373 (1987).
[59] M. Lattuada, F. Riggi, D. Vinciguerra, C. Spitaleri, G. Vourvopoulos, Dj. Miljanić, and E. Norbeck, Z. Phys. A **330**, 183 (1986).
[60] S. Blagus, C. Blyth, G. Calvi, O. Karban, M. Lattuada, Dj. Miljanić, F. Riggi, C. Spitaleri, and M. Zadro, Z. Phys. A **337**, 297 (1990).
[61] N. Soić, D. Calí, S. Cherubini, E. Costanzo, M. Lattuada, M. Milin, Dj. Miljanić, S. Romano, C. Spitaleri, and M. Zadro, Eur. Phys. J. A **3**, 303 (1998).
[62] H. W. Becker, C. Rolfs, and H. P. Trautvetter, Z. Phys. A **327**, 341 (1987).
[63] F. C. Barker, Nucl. Phys. **A707**, 277 (2002).